ARID ZONE JOURNAL OF ENGINEERING, TECHNOLOGY & ENVIRONMENT
AZOJETE September 2026. Vol.22(3):846-862
Published by the Faculty of Engineering, University of Maiduguri, Maiduguri, Nigeria.
**Print ISSN: 1596-2490, Electronic ISSN: 2545-5818**
https://doi.org/10.63958/AZOJETE/2026/22/03/024
www.azojete.com.ng

ORIGINAL RESEARCH ARTICLE

# OPTIMIZATION OF CFRP AND STEEL REINFORCED CONCRETE NUCLEAR SHELL ROOFS USING EXCEL SOLVER

**K.U. Unamba[1*], O.S. Abejide[2], J.M. Kaura[2], A. Lawan[2]**

[1]*Department of Civil Engineering, Taraba State University, Jalingo, Nigeria*
[2]*Department of Civil Engineering, Ahmadu Bello University, Zaria, Nigeria*
**Corresponding author email: udokanma@tsuniversity.edu.ng*

**ARTICLE INFORMATION**

**Received: 4th July 2026**
**Revised: 14th July 2026**
**Accepted: 16th July 2026**

**Keywords:**
*Structural optimization*
*Generalized reduced gradient*
*Shell roofs*
*CFRP reinforcement*
*Reliability analysis*

## ABSTRACT

*Nuclear containment shell roofs must remain leak tight over service lives approaching 100 years, yet they are difficult to inspect and impossible to replace, so the corrosion of steel reinforcement is a recognised durability concern. Carbon fibre reinforced polymer (CFRP) reinforcement is immune to electrochemical corrosion but has a lower modulus and no ductility, so its design must be reformulated rather than substituted. This study developed an optimization framework that designed the reinforcement of a nuclear shell roof with steel and with CFRP on a strictly common basis; corrosion resistance motivated the comparison, but its long-term benefit was not quantified here. The dome was idealised as a spherical cap, the membrane and edge bending forces were derived analytically, and the weighted material consumption was minimised over the shell thickness and reinforcement ratio subject to strength, crack width, deflection, buckling, durability and severe accident constraints drawn from the governing Eurocode 2 provisions. The optimisation model was solved in Microsoft Excel Solver with the generalised reduced gradient algorithm, the shell solution was verified against a finite element analysis in Abaqus, and the reliability of each optimum was computed by the first order reliability method (FORM) and checked by Monte Carlo simulation (MCS) in Python. The steel optimum was a 0.31 m shell with a 1.18% reinforcement ratio governed jointly by strength and crack control; the CFRP optimum was a 0.32 m shell with a 0.52% ratio governed by crack control alone, a 56% reduction in reinforcement ratio at essentially the same thickness. The analytical forces agreed with the finite element results to within 3%. FORM returned reliability indices of 4.44 for the steel strength state and 3.76 for the CFRP crack width state, and MCS confirmed them with failure probabilities of 4.4 × $10^{-6}$ from 50 million samples and 1.0 × $10^{-4}$ from 10 million samples, equivalent to indices of 4.45 and 3.72. Both designs satisfied their respective ultimate and serviceability targets for nuclear structures, and the optimisation model itself was run in a standard spreadsheet in which every cell and relationship remained open to audit.*



## 1.0 Introduction

Reinforced concrete shell roofs form the principal containment barrier of many nuclear facilities. The nuclear application is chosen deliberately, because it concentrates the demands that make the reinforcement material decision consequential: a design life approaching 100 years, a strict leak tightness requirement expressed through crack control, accident pressure and thermal conditions that ordinary roofs never see, and a regulatory environment that requires every design assumption to be auditable. Steel reinforcement is limited in this setting by corrosion, which is time dependent and progressive, so the safety margin of a steel reinforced containment declines over the service life once carbonation or chloride ingress initiates the process (Benmokrane *et al.*, 2017). Carbon fibre reinforced polymer (CFRP) reinforcement is immune to electrochemical corrosion but is brittle and has a lower elastic modulus, so the design cannot simply substitute one bar for another (ACI Committee 440, 2015; British Standards Institution, 2004). A rational choice between the two systems requires a framework that couples shell analysis with formal optimisation under the relevant code provisions and treats both materials on identical terms.

Four strands of the optimisation literature border the problem without solving it. The first is the cost or weight optimisation of flexural members such as beams, columns and frames, which is mature, includes gradient based and metaheuristic solutions, and has recently been extended to satisfy ultimate and serviceability limit states simultaneously (Afzal *et al.*, 2020; Juliani and Gomes, 2021; Larsen *et al.*, 2024; Mergos, 2018; Pierott *et al.*, 2021). The second is the form finding and topology optimisation of shells, in which the surface geometry is varied to reduce bending while the reinforcement is treated, if at all, as a subsequent calculation (Zingoni, 2018). The third is reliability based and performance based design optimisation, reviewed for a range of structural types (Abejide, 2014; Saraswat and Ghosh, 2024; Sykora *et al.*, 2017). The fourth is the optimisation of FRP systems, which has concerned the strengthening or confinement of existing members rather than the internal reinforcement of new shells (Firouzi *et al.*, 2021; Hollaway, 2010; Spinella, 2025). Few studies have formulated the reinforcement design of a doubly curved containment shell of fixed geometry as a single optimisable model, and the authors are not aware of one that brings optimised steel and optimised CFRP designs of such a shell to a controlled comparison.

The gap persists because the governing mechanics differ from those the existing formulations assume. A pressurised containment shell is governed by biaxial membrane tension modified by a localised edge bending disturbance, not by the bending moment of a one-dimensional member, so the demand model, the resistance model and the binding serviceability limit all differ in kind from the flexural case (Billington, 1982; Wu *et al.*, 2015). The present formulation therefore evaluates the demand as the biaxial membrane force field at the governing meridional location augmented by the edge bending interaction, writes the serviceability constraints for the cracked biaxially stressed section with modulus dependent crack and deflection relationships, and represents the two reinforcement systems through a single parameterised constraint set that differs only where the materials genuinely differ. Table 1 summarises this position against the four strands, with representative sources for each. The novelty is one of formulation and application rather than of algorithm.

**Table 1:** Position of the present formulation against existing optimisation strands

| Feature | Flexural RC optimization | Shell form finding | FRP strengthening | Present framework |
|---|---|---|---|---|
| Structural action | Bending of members | Membrane via shape | Confinement or flexure | Biaxial membrane plus edge bending |
| Design variables | Section size, steel area | Surface geometry | Layers, wrap extent | Thickness, reinforcement ratio |
| Governing limit | Strength | Bending energy | Strength or ductility | Crack control and strength |
| Steel and CFRP parity | Rare | Not addressed | FRP only | Strictly parallel |
| Reliability measure | Sometimes | No | Sometimes | FORM and Monte Carlo |
| Implementation | Bespoke or metaheuristic | Specialised FE | Bespoke | Spreadsheet, auditable |
| Representative sources | Afzal *et al.* (2020); Pierott *et al.* (2021) | Zingoni (2018) | Hollaway (2010); Firouzi *et al.* (2021) | This study |

The spreadsheet implementation is itself part of the contribution. Much recent optimisation of reinforced concrete relies on metaheuristic algorithms and bespoke computational environments that are inaccessible to many practising engineers, particularly in resource constrained settings, and that resist independent audit (Rao, 2019; Zhu *et al.*, 2021). A framework that delivers code consistent optima within a standard spreadsheet lowers that barrier, and in a regulated nuclear context the visibility of every cell and relationship is an advantage in its own right. The objective of the paper is therefore to develop the optimisation framework, to verify it against finite element analysis, to present the serviceability formulations explicitly, and to quantify the reliability of the optimised steel and CFRP designs. The scope needs stating plainly. The framework sizes the global reinforcement of the dome; the steel liner and its anchorage, prestressing, leak rate acceptance testing, post accident integrity assessment and the wider licensing provisions are parts of containment design that lie outside it and are handled by the dedicated procedures of the applicable nuclear codes (IAEA, 2016). The nuclear setting supplies the constraint set for the optimisation, the crack width limit, the accident pressures and the reliability targets, rather than a complete containment design. Equally, the corrosion argument that motivates CFRP is not tested here: corrosion initiation and propagation, the associated decline of the steel reliability index and the life cycle cost are not modelled, so the durability advantage of CFRP enters this study as a motivation, not as a demonstrated result. The reliability reported is that of each design at the start of service; the time variant analysis of the corroding steel design is identified as the necessary next stage of the work.

## 2. Materials and Method

This was a theoretical and computational study. The method had five parts, presented in turn: the shell idealisation and its analytical solution, the material models, the actions and nuclear specific requirements, the optimisation formulation, and the solution, verification and reliability procedures. The design problem was to find, for a containment shell roof of given geometry and loading, the shell thickness and reinforcement configuration that minimise material consumption while satisfying all strength, serviceability, stability and durability requirements, separately for steel and for CFRP so that the two optima can be compared. The problem was a smooth single objective nonlinear program with 2 continuous variables and a bounded feasible region, which suited the generalised reduced gradient algorithm. The modelling assumptions were that the shell was thin, so transverse shear deformation was neglected away from the edge; that the middle surface was spherical and of uniform thickness; and that the materials followed their code idealisations, elastic perfectly plastic for steel and linear elastic to brittle rupture for CFRP. The framework sized the global reinforcement of the dome away from penetrations, thickenings and the liner, which were detailed separately by local analysis in practice, and it was intended for preliminary global sizing and for checking more elaborate analyses rather than for the complete design of a containment.

### 2.1 Shell Idealisation and Structural Analysis

The roof was idealised as a spherical cap of uniform thickness t supported on a ring beam, representing the domed roof of a cylindrical containment. Figure 1 shows the geometry and coordinate system and Figure 2 the membrane stress resultants on a shell element; the reference parameters are listed in Table 2 with their sources. For a spherical shell of radius R under a uniform vertical load q per unit area of the middle surface, equilibrium of the cap above a parallel circle gives the meridional and hoop membrane forces per unit length (Timoshenko and Woinowsky-Krieger, 1959; Billington, 1982) as

$$N\varphi = -\frac{qR}{1 + \cos\varphi} \qquad 1$$

$$N_\theta = qR\left(\frac{1}{1 + \cos\varphi} - \cos\varphi\right) \qquad 2$$

where ϕ is the meridional angle from the crown. Under an internal pressure p the membrane forces in the spherical region are equal in both directions (Timoshenko and Woinowsky-Krieger, 1959),

$$N_\varphi = N_\theta = \frac{pR}{2} \qquad 3$$

The bracketed term of Equation 2 changes sign near 51 degrees from the crown, below which the hoop force is compressive and above which it is tensile, while under pressure both forces are tensile and uniform, so the pressure case governs the reinforcement over most of the dome. The total design tensile membrane force per unit length at the governing location, $N_{Ed}$, combines the factored contributions of the relevant actions. The membrane solution does not satisfy the boundary condition at the ring beam, where radial expansion is restrained; the incompatibility is resolved by a self equilibrating edge bending field that decays over the characteristic length (Calladine, 1983)

$$L_b = \frac{\sqrt{Rt}}{[3\,(1-\nu^2)]^{1/4}} \qquad 4$$

where ν is the Poisson ratio of concrete, taken as 0.2. Within roughly one decay length of the edge the bending moment and the associated reinforcement demand are significant; the optimisation represents this zone by evaluating the combined axial force and bending moment at the boundary and requiring the section to satisfy the corresponding interaction, so the reinforcement suffices at the most demanding location.

Three simplifications of the idealisation deserve emphasis. Real containment roofs carry penetrations, equipment hatches, anchors and local thickenings that redistribute forces around them; the uniform spherical cap excludes these, which is acceptable for the global sizing intended here but not for local design, and Section 3.6 recorded it as a limitation. The ring beam was represented as a partial radial and rotational restraint rather than derived from a specific beam section, because the edge disturbance decayed within the characteristic length of Equation 4 whatever the exact stiffness; the finite element model of Section 2.5 calibrated this restraint to the stiffness of a supporting wall, and the sensitivity of the edge reinforcement demand to that calibration has not been mapped, which was likewise recorded as a limitation. The uniform thickness assumption followed the practice of preliminary shell sizing (Billington, 1982; Zingoni, 2018), and any edge thickening adopted in detailed design only increased the margin at the location the interaction check governed.

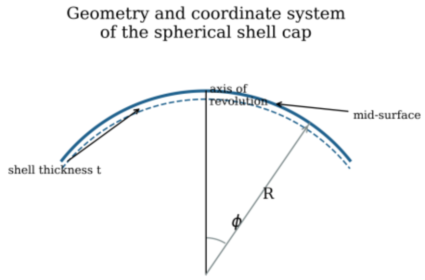


**Figure 1:** Geometry and coordinate system of the spherical shell cap

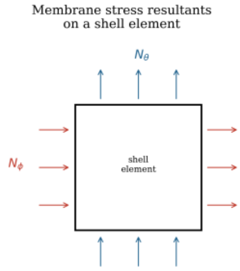


**Figure 2:** Membrane stress resultants on a shell element

**Table 2:** Reference geometry, material and durability parameters

| Parameter | Symbol | Value | Unit | Source |
|---|---|---|---|---|
| Base diameter | 2a | 40.0 | m | Typical containment span (Zingoni, 2018) |
| Radius of curvature | R | 25.0 | m | Geometry of the reference dome |
| Initial shell thickness | t | 0.30 | m | Zingoni (2018) |
| Concrete strength (characteristic) | f(ck) | 45 | MPa | BS EN 1992-1-1 (2004), Table 3.1 |
| Concrete secant modulus | E(cm) | 36 | GPa | BS EN 1992-1-1 (2004), Table 3.1 |
| Steel yield strength (characteristic) | f(yk) | 500 | MPa | BS EN 1992-1-1 (2004), Annex C |
| Steel elastic modulus | E(s) | 200 | GPa | BS EN 1992-1-1 (2004), cl. 3.2.7 |
| CFRP tensile strength (characteristic) | f(fk) | 2300 | MPa | ACI 440.1R-15 (2015) |
| CFRP elastic modulus | E(f) | 165 | GPa | ACI 440.1R-15 (2015) |
| Concrete cover | c | 0.050 | m | BS EN 1992-1-1 (2004), cl. 4.4.1 |
| Crack width limit (leak tightness) | w(lim) | 0.20 | mm | BS EN 1992-3 (2006), cl. 7.3.1 |
| Design life | t(L) | 100 | years | Nuclear service requirement (IAEA, 2016) |

### 2.2 Material Models

Concrete follows the parabola rectangle relationship in compression of BS EN 1992-1-1 clause 3.1.7, with design strength (British Standards Institution, 2004, cl. 3.1.6)

$$f_{cd} = \frac{\alpha_{cc} f_{ck}}{\gamma_c} \qquad 5$$

where $\alpha_{cc}$= 0.85 is the long term strength factor and $\gamma_c$ = 1.5 the concrete partial factor. Steel is elastic perfectly plastic with design yield strength (British Standards Institution, 2004, cl. 3.2.7)

$$f_{yd} = \frac{f_{yk}}{\gamma_s} \qquad 6$$

where $\gamma_s$ = 1.15. CFRP is linear elastic to brittle rupture with design tensile strength (ACI Committee 440, 2015)

$$f_{fd} = \frac{\eta_{env} f_{fk}}{\gamma_f} \qquad 7$$

where $\eta_{env}$ = 0.85 is the environmental reduction factor and $\gamma_f$ = 1.5 the material partial factor. Because CFRP does not yield, the ultimate strain is limited to the design rupture strain, and the sustained stress under the quasi-permanent combination is limited to 0.55 $f_{fk}$ to guard against creep rupture, consistent with the reported retention of 70 to 90% of the initial strength of carbon systems after 50 years under load (Bischoff, 2005; Wu *et al.*, 2015; Ashrafi *et al.*, 2022). Fatigue was not constrained because the dominant actions, self-weight and the rare accident pressure, were essentially static. Elevated accident temperature was covered conservatively by η(env) and the accident thermal gradient in the load combinations. Radiation damage to the matrix was not modelled quantitatively because design relationships for the low fluence at a roof remote from the core were not yet codified; it was addressed by detailing and shielding (International Atomic Energy Agency, 2016).

Two of these positions needed explicit support. The environmental reduction factor of 0.85, the indoor exposure value of ACI 440.1R-15 (2015), was not critical to the optimum: because the CFRP design proved to be governed by crack width alone and retained a 33% margin on the strength constraint, reducing the factor to 0.70 and would raise the strength utilization only to about 0.81 and leave the reported optimum unchanged, so the design was insensitive to this factor across its plausible range. The treatment of accident temperature was conservative rather than detailed: the full accident differential was applied as a linear gradient in the load combinations, which bounded the restrained curvature demand of a thin cracked section because the additional nonlinear component of a real transient profile was self-equilibrating and is relieved once the section cracks, the position taken for thermal actions on concrete sections in BS EN 1992-1-2 (2004). The omission of radiation effects remained a genuine restriction of scope for the nuclear application, and it was carried into the limitations of Section 3.6 rather than treated as resolved.

### 2.3 Actions and Nuclear Specific Requirements

The actions, their characteristic values and their partial factors are listed in Table 3 with their sources. They are combined at the ultimate limit state under the combination rules of BS EN 1990 (2002) as implemented in BS EN 1992-1-1 clause 2.4 and, for the containment function, BS EN 1992-3 (British Standards Institution, 2004, 2006). The governing ultimate combination was dominated by self weight and the accident internal pressure. The design basis accident combined the accident pressure with the permanent actions and the accident thermal gradient; the severe accident was a separate check of characteristic resistance against a higher pressure with unit partial factors. Leak tightness was represented by the 0.20 mm crack width limit of BS EN 1992-3 clause 7.3.1, which proved to govern the CFRP design. The serviceability combinations used characteristic and quasi permanent values as appropriate to the deflection and crack checks.

The pressure magnitudes of Table 3 are representative rather than project specific, and were used as such: the 0.40 MPa operating and 0.52 MPa design basis accident pressures sat within the 0.3 to 0.5 MPa band reported for large dry containments, and the 0.62 MPa severe accident check followed the practice of testing characteristic resistance against a pressure well above the design basis (IAEA, 2016; Sykora *et al.*, 2017). Because the membrane tension was proportional to the product of pressure and radius, a project specific pressure rescaled the demand without changing the structure of the model, and the sensitivity study of Section 3.3 covered the influence of such rescaling through the load variations. The accident thermal action was applied as a uniform linear gradient of 60 °C through the thickness for the reason set out in Section 2.2: the linear component controlled the restrained curvature of a thin shell, and the self equilibrating remainder of a real nonlinear transient was relieved on cracking, so the uniform gradient bounded the design effect.

**Table 3:** Characteristic actions and partial factors

| Action | Characteristic value | ULS factor | Source |
|---|---|---|---|
| Self weight (t = 0.30 m, 24 kN/m3) | 7.2 kN/m$^2$ | 1.35 | BS EN 1991-1-1 (2002); BS EN 1992-1-1 (2004) |
| Superimposed dead load | 1.5 kN/m$^2$ | 1.35 | BS EN 1991-1-1 (2002) |
| Imposed and maintenance load | 1.0 kN/m$^2$ | 1.50 | BS EN 1991-1-1 (2002) |
| Operating internal pressure | 0.40 MPa | 1.35 | Plant design condition (IAEA, 2016) |
| Accident internal pressure | 0.52 MPa | 1.20 | Design basis accident (IAEA, 2016) |
| Severe accident pressure (check) | 0.62 MPa | 1.00 | Severe accident condition (IAEA, 2016) |
| Thermal gradient (accident) | 60 °C through thickness | 1.00 | IAEA (2016) |
| Seismic (equivalent static) | 0.18 g | 1.00 | Site design spectrum (IAEA, 2016) |

### 2.4 Optimisation Formulation

Two decision variables were adopted: the shell thickness t and the reinforcement ratio ρ, defined as the reinforcement area per unit length divided by the gross section area per unit length. These two variables controlled everything that determined feasibility and consumption. The thickness fixed the concrete volume, the stiffness governing deflection and buckling, and the cover available for durability; the ratio fixed the tensile resistance and the crack width. Bar diameter and spacing were detailing choices made after optimisation to realise the computed ratio, entering the model only through the crack spacing coefficients of Equation 13. The geometry was fixed by the containment function and the concrete grade was selected from standard grades, so both were treated as design conditions and examined parametrically rather than optimised. The objective was the weighted material consumption

Restricting the optimisation to these two continuous variables was deliberate. Bar diameter, spacing and layer arrangement were discrete quantities whose introduction turned the smooth program into a mixed integer one without changing the governing trade off, since they influenced the model only through the crack spacing coefficients; they were therefore assigned after optimisation, and Section 3.5 demonstrated that the computed ratios were realisable with standard bar sizes at code compliant spacings.

$$Minimise\ W = \rho_c V_c + k\rho_r V_r \tag{8}$$

where $\rho_c$ and $\rho_r$ are the densities of concrete and reinforcement, $V_c$ and $V_c$ their volumes, and k a weighting factor expressing the relative significance of reinforcement mass. The reference value k = 5 restored the reinforcement term, which was otherwise about 30 times smaller than the concrete term, to a comparable influence on the objective; because this was an order of magnitude calibration, the dependence of the optimum on k was quantified over the range 1 to 20 in Section 3.3. The strength constraints required the design tensile resistance to meet the governing design tension $N_{Ed}$ at the critical location, for steel and CFRP respectively (British Standards Institution, 2004, cl. 6.1; ACI Committee 440, 2015):

The weighting was a scaling device, not an economic claim. A cost objective replaced k by the ratio of reinforcement to concrete price per unit volume, and a carbon objective by the ratio of the emission factors; both ratios vary by market and by year, which was why neither was hard coded. What Section 3.3 shows is that the optimum sits on the intersection of binding constraints and moves by less than 4% in thickness and 3% in ratio as k varies from 1 to 20, so any cost or carbon weighting whose effective ratio falls in that wide range returns the same design; the mass basis was retained because it keeps the objective auditable without market data.

$$A_s f_{yd} \geq N_{Ed} \tag{9}$$

$$A_f f_{fd} \geq N_{Ed} \tag{10}$$

where $A_s$ and $A_f$ are the reinforcement areas per unit length. Stability under the compressive meridional force is checked against the classical critical pressure of a spherical shell (Timoshenko and Woinowsky-Krieger, 1959)

$$p_{cr} = \frac{2E_{cm}\left(\frac{t}{R}\right)^2}{[3\,(1-\nu^2)]^{0.5}} \tag{11}$$

reduced by an imperfection knockdown factor of 0.20 following the lower bound formulation for spherical shells (Wagner *et al.*, 2018; Blachut, 2016). Durability requires the cover to meet the exposure class minimum and the sustained reinforcement stress to remain below its limit. The crack width under the serviceability combination follows BS EN 1992-1-1 clause 7.3.4 (British Standards Institution, 2004),

$$w_k = s_{r,max}\,(\varepsilon_{sm} - \varepsilon_{cm}) \leq w_{lim} \tag{12}$$

$$s_{r,max} = k_{3\,c} + k_1 k_2 k_4 \frac{\varphi_b}{\rho_{eff}} \tag{13}$$

$$\varepsilon_{sm} - \varepsilon_{cm} = \frac{[\sigma_r - k_t\, f_{ct,eff}\,(1 + \alpha_e\,\rho_{eff})]}{E_r}\,\frac{1}{\rho_{eff}} \geq \frac{0.6\,\sigma_r}{E_r} \tag{14}$$

where c is the cover, $\varphi_b$ the bar diameter, $\rho_{eff}$ the effective reinforcement ratio in the tension zone, $\sigma_r$ the reinforcement stress under the serviceability combination, $E_r$ the reinforcement modulus, $\alpha_e$ the modular ratio, $f_{ct,eff}$ the effective concrete tensile strength, $k_t$ the load duration factor, and $k_1$ to $k_4$ bond and strain distribution coefficients, with $k_1$ increased for the smoother surface of FRP bars (ACI Committee 440, 2015; fib, 2007). Because the strain term is inversely proportional to $E_r$, a lower modulus reinforcement carries a larger strain at a given stress and therefore a wider crack unless a larger area reduces the stress; the 0.20 mm limit thus fixes the CFRP area at the serviceability state. The apex deflection is limited to span/500 through the tension stiffening interpolation of BS EN 1992-1-1 clause 7.4.3, with the coefficient β reduced for FRP following the calibration of Bischoff (2005):

$$\delta = \zeta\, \delta_{II} + (1 - \zeta)\, \delta_I \leq \frac{span}{500} \qquad 15$$

$$\zeta = 1 - \beta \left(\frac{M_{cr}}{M}\right)^2 \qquad 16$$

where $\delta_I$ and $\delta_{II}$ are the uncracked and fully cracked deflections, $\zeta$the interpolation coefficient, and M and $M_{cr}$ the applied and cracking moments. Table 4 summarises the complete model.

**Table 4:** Decision variables, objective and constraints of the optimisation model

| Element | Description |
|---|---|
| Decision variables | Shell thickness t; reinforcement ratio ρ (steel or CFRP) |
| Objective | Minimise weighted material consumption W, Equation 8 |
| Strength | Design resistance at least the design action effect, Equations 9 and 10 |
| Crack width | $w_k$ not exceeding 0.20 mm for leak tightness, Equations 12 to 14 |
| Deflection | Apex deflection not exceeding span/500, Equations 15 and 16 |
| Stability | Compressive membrane force not exceeding 0.20 $p_{cr}$, Equation 11 |
| Durability | Cover at least the exposure minimum; sustained stress below its limit |
| Severe accident | Characteristic resistance at least the severe accident demand |
| Side constraints | 0.20 m ≤ t ≤ 0.45 m; ratio within practical bounds |

### 2.5 Solution Procedure, Verification and Reliability Methods

The model was implemented in a Microsoft Excel workbook with a parameter block, an input block holding the decision variables, an analysis block encoding Equations 1 to 16, and a results block from which Solver reads; the workbook is available from the corresponding author. Solver minimises the objective cell with the generalised reduced gradient (GRG) nonlinear engine, central differencing and multistart from 10 starting points to guard against local optima (Lasdon *et al.*, 1978). The procedure, shown in Figure 3, was identical in structure for the two systems, differing only in the material model and the reinforcement specific constraints, which was what made the comparison controlled.

GRG was preferred to evolutionary, genetic, particle swarm and sequential quadratic programming alternatives on the character of the problem rather than on convenience: the program was smooth, had two continuous variables and a small bounded feasible region, which was the setting in which a gradient method converged rapidly to a stationary point and population based metaheuristics offered no accuracy advantage while costing far more function evaluations (Rao, 2019; Zhu *et al.*, 2021). The exposure of GRG to local optima, the one respect in which population methods could help, was covered by the multistart from 10 dispersed starting points, and the uniqueness evidence of Section 3.1 confirms that a single optimum was found; a formal benchmarking of solver families on this problem would therefore measure computing time rather than design outcome.

Verification and validation were distinguished throughout: verification asked whether the equations were solved correctly, validation asked whether the model represented the physical problem. Three procedures addressed them. First, the analytical shell solution was verified against an independent finite element analysis of the reference dome in Abaqus/Standard, using 4 node doubly curved thin shell elements with reduced integration and hourglass control (element S4R, 6 degrees of freedom per node). The mesh was refined toward the ring beam so that at least 8 elements fell within one decay length $L_b$; a convergence study on 7 meshes from 320 to 11520 elements showed the peak edge meridional force rising monotonically to a converged 158.0 kN/m, with the change between successive meshes falling to 0.24% at 5120 elements, which was adopted. The base was represented by a radial spring calibrated to the stiffness of the supporting wall plus vertical restraint, reproducing the partial fixity that generates the edge bending field. Second, a one at a time sensitivity analysis varied the concrete grade, rise to span ratio, reinforcement modulus, live load, creep coefficient and material partial factor by plus and minus 10% about their reference values, and the optimum was recomputed for k = 1, 2, 5, 10, 15 and 20. Third, the reliability of each optimised design was assessed against its governing limit state: the strength state of Equation 9 for steel and the crack width state of Equation 12 for CFRP.

The reliability computations were coded in Python, since the iterative transformation not practical in a spreadsheet. The first order reliability method (FORM) transformed the non normal variables to equivalent normals at the current point by the Rackwitz and Fiessler (1978) procedure and located the design point with the Hasofer and Lind (1974) iteration scheme, the reliability index β being the distance from the origin to the design point in standard normal space and the squared direction cosines giving the contribution of each variable to the variance of the margin. FORM was approximate because it linearized the limit state at the design point, so it was checked by crude Monte Carlo simulation (MCS), which estimated the failure probability P(f) directly as the proportion of samples with a negative margin and was exact within sampling error (Melchers and Beck, 2018); MCS therefore served as the benchmark that validated the FORM approximation, while FORM supplied the sensitivity factors that MCS did not.

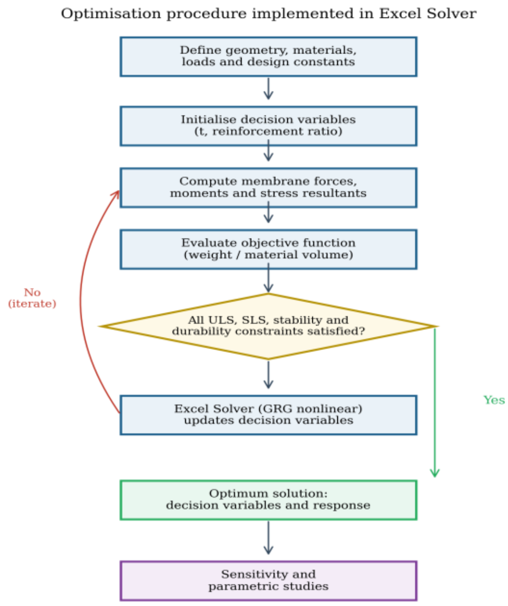


**Figure 3:** Optimisation procedure implemented in Microsoft Excel Solver

The limit state functions were stated explicitly, because both methods operated on them directly. For the steel design the governing state was strength, with performance function

$$g_1(X) = M_R A_s f_y - (N_g + N_p) \tag{17}$$

where $M_R$ is the resistance model factor, $A_s$ the reinforcement area per unit length, $f_y$ the yield strength, and $N_g$ and $N_p$ the membrane tensions produced at the governing location by the permanent actions and by the accident pressure of Table 3. For the CFRP design the governing state is crack width, with performance function

$$g_2(X) = w_{lim} - M_w w_k(X) \tag{18}$$

where $w_{lim}$ is the 0.20 mm limit, $M_w$ the crack model factor, and $w_k$(X) the crack width of Equations 12 to 14 evaluated with the random sustained tension, elastic modulus and effective depth in place of their design values. Failure corresponded to a performance function value at or below zero in either state. The basic variables were treated as statistically independent, so their joint probability density was the product of the marginal densities listed in Table 5. The load and resistance quantities in that table were the same quantities that appeared in the optimisation model: each characteristic value and partial factor of Table 3 was replaced by the mean, coefficient of variation and distribution type appropriate to a probabilistic description (JCSS, 2001), so the reliability analysis assessed exactly the designs the optimisation produced.

For the simulation, each sample of the basic variables was generated by drawing independent standard uniform numbers from the Mersenne Twister generator of NumPy and transforming them to the marginal distributions by the inverse of each cumulative distribution function, the normal and lognormal variables through the standard library transforms and the Gumbel variables through the closed form inverse of the Gumbel distribution with location and scale fitted from the mean and coefficient of variation; independence was preserved because each variable was drawn from its own stream. The failure probability was estimated by the indicator average

$$P_f = \frac{1}{N}\sum I[g(x_j) \leq 0] \quad 19$$

where the indicator I[ ·] equals one when the sampled performance function is not positive and zero otherwise, and $N$ is the number of samples. The standard error of the estimate is

$$s.e.(P_f) = \sqrt{\frac{P_f(1-P_f)}{N}} \quad 20$$

so each estimate is reported with a 95% confidence interval of plus or minus 1.96 standard errors. For comparison with FORM, each estimate is expressed as an equivalent reliability index through the inverse standard normal transformation

$$\beta = -\Phi^{-1}(P_f) \quad 21$$

The sample sizes, 50 million for the steel state and 10 million for the CFRP state, were set from Equation 20 so that the expected number of failures exceeded 200 and 1000 respectively at the anticipated probabilities, which holds the coefficient of variation of the estimates below about 7% and 3%. The computations are vectorised in NumPy, and both runs were completed in under five minutes on an ordinary desktop computer with four processor cores and 16 GB of memory, so the sample sizes carried no unusual computational cost.

The governing design tension $N_{Ed} = 1.35 \times 120 + 1.20 \times 315 = 540\ kN/m$ is consistent with the characteristic values of Table 5, and the crack model factor had a mean well below unity because the code formula predicted an upper fractile rather than a mean crack width (Fib, 2007).

**Table 5:** Basic random variables for the reliability analysis and their counterparts in the design model

| Random variable | Design model counterpart (Table 3) | Distribution | Mean | COV (%) | Source |
|---|---|---|---|---|---|
| Resistance model factor $M_R$ | Modelling uncertainty of Equation 5 | Lognormal | 1.00 | 5 | JCSS (2001) |
| Steel yield strength $f_y$ (MPa) | Characteristic strength 500 MPa | Lognormal | 560 | 5 | JCSS (2001) |
| Permanent tension $N_g$ (kN/m) | Self weight and finishes, factor 1.35 | Normal | 120 | 8 | JCSS (2001) |
| Accident pressure tension $N_p$ (kN/m) | Accident pressure 0.52 MPa, factor 1.20 | Gumbel | 300 | 8 | Sykora *et al.* (2017) |
| Crack model factor $M_w$ | Model uncertainty of Equation 12 | Lognormal | 0.70 | 18 | fib (2007); JCSS (2001) |
| Sustained to characteristic tension ratio | Quasi permanent combination factor | Gumbel | 0.63 | 10 | JCSS (2001) |
| CFRP elastic modulus $E_f$ (GPa) | Modulus in Equations 12 and 14 | Normal | 165 | 4 | Ashrafi *et al.* (2022) |
| Effective depth $d$ (m) | Thickness less cover and half bar | Normal | 0.26 | 5 | JCSS (2001) |

## 3. Results and Discussion

### 3.1 Optimum Designs

The steel optimisation returned an optimum thickness of 0.31 m and a reinforcement ratio of 1.18%, with both the strength and the crack width constraints active at the optimum. The CFRP optimisation returned a thickness of 0.32 m and a ratio of 0.52%, with the crack width constraint alone active and the strength constraint satisfied at a utilisation of about 0.67. The governing design tension at the critical location was 540 kN/m for both designs, since it depended on geometry and loading rather than on the reinforcement. Propagating the parameter variability of Section 3.3 through the model places one standard deviation bands of about plus or minus 0.10% on the steel ratio, 0.05% on the CFRP ratio and 0.02 m on the thicknesses; Table 6 summarises the optima with these bands.

**Table 6:** Optimum designs with estimated sensitivity bands (1 standard deviation)

| Quantity | Steel design | CFRP design |
|---|---|---|
| Optimum thickness t (m) | 0.31 ± 0.02 | 0.32 ± 0.02 |
| Optimum reinforcement ratio (%) | 1.18 ± 0.10 | 0.52 ± 0.05 |
| Governing design tension $N_{Ed}$ (kN/m) | 540 | 540 |
| Active constraints at optimum | Strength and crack width | Crack width only |
| Strength utilisation at optimum | 1.00 | 0.67 |

Three inferences follow. First, the steel design was efficient in the classical sense, with neither the strength nor the crack requirement carrying spare margin, whereas the CFRP design could not exploit the strength of its material: a third of the tensile capacity was unusable because the 0.20 mm leak tightness limit fixes the area first. That a third of the capacity was priced away by a crack formula calibrated on steel reinforced sections is itself a finding: the bond coefficient and the fixed 0.20 mm limit of Equations 12 to 14 were not derived for FRP bar surfaces, so how representative the formula is of FRP containment sections remains an open experimental question (fib, 2007; ACI Committee 440, 2015), and Section 3.4 shows the same model uncertainty dominating the CFRP reliability. Any change that relaxes crack control, a coating that improves bond or a limit revised for corrosion resistant reinforcement, would therefore benefit CFRP directly and steel hardly at all. Second, the CFRP ratio is 56% below the steel ratio at essentially the same thickness, which showed that the high strength of the material did translate into less reinforcement, just not in proportion to the strength ratio of the two materials. Third, the optima compared sensibly with the published record: the steel ratio of 1.18% lies within the 0.8 to 1.6% band reported for containment and large span concrete domes (Zingoni, 2018), the CFRP ratio of 0.52% within the 0.4 to 0.9% band for FRP designs governed by serviceability (Spinella, 2025), and the pattern of a serviceability governed FRP optimum reproduces what flexural optimisation studies of FRP members report (Bischoff, 2005; Pierott *et al.*, 2021), while spreadsheet nonlinear programming of RC members had likewise been found to converge in a comparable number of iterations (Zhu *et al.*, 2021). The present results extended that record from flexural members to a biaxially stressed shell.

The optima were also unique and cheap to find. All 10 multistart runs for each system converged to the same point, with the spread in the final objective below 0.3% and in the final variables below 0.5%, in 12 iterations on average for steel and 11 for CFRP and in under 2 s per run on an ordinary desktop computer. Stationarity was confirmed by perturbing each variable about the converged point and verifying that the objective did not decrease within the feasible region, the check that stood in for a solver benchmarking exercise on a smooth two variable program, as argued in Section 2.5. Figure 4 shows the objective histories, which are smooth and monotonic, so the framework behaves as a routine design tool that needs no expert tuning.

### 3.2 Verification and Validation

Implementation correctness was verified by reproducing closed form limiting cases: the membrane forces of a complete sphere under internal pressure matched Equation 3 exactly, and the buckling pressure matched the classical critical pressure within the knockdown tolerance. The finite element comparison then tests the analytical demand model itself. Figure 5 compares the meridional and hoop membrane forces along the meridian from Equations 1 and 2 with the converged Abaqus values, and Table 7 gives the errors at representative angles. The agreement is within 3% up to about 45 degrees from the crown, rising to between 4 and 6% within roughly one decay length of the ring beam, where the numerical model captures the edge bending disturbance that the membrane solution excludes. The analytical solution also reproduces the change of sign of the hoop force near 51 degrees. The larger edge deviation was expected and was precisely the region the framework treated separately through the boundary force and moment interaction, so the demand model was accurate where it was relied upon.

Validation against independent evidence is summarised in Table 8: the optimum thickness to span ratio, both reinforcement ratios, the knockdown factor and both reliability indices fall within the ranges published for comparable shells and reliability targets. Falling inside published bands demonstrated plausibility rather than validation in the strict sense, and no experimental test of a comparable shell entered the comparison, because published experiments on pressurised containment models are scarce; the validation offered here is therefore necessarily indirect. Table 8 accordingly reports, alongside each range, the position of the present value within it: the six quantities lie at positions between 0.24 and 0.95 of their bands, none at an extreme, and the serviceability index sits high in its band precisely because the crack constraint was the binding one. The quantitative weight of the section rests on the finite element comparison of Table 7, which tests the demand model directly; the literature comparison then checked that the optimised designs were not outliers among built and studied shells and published reliability targets.

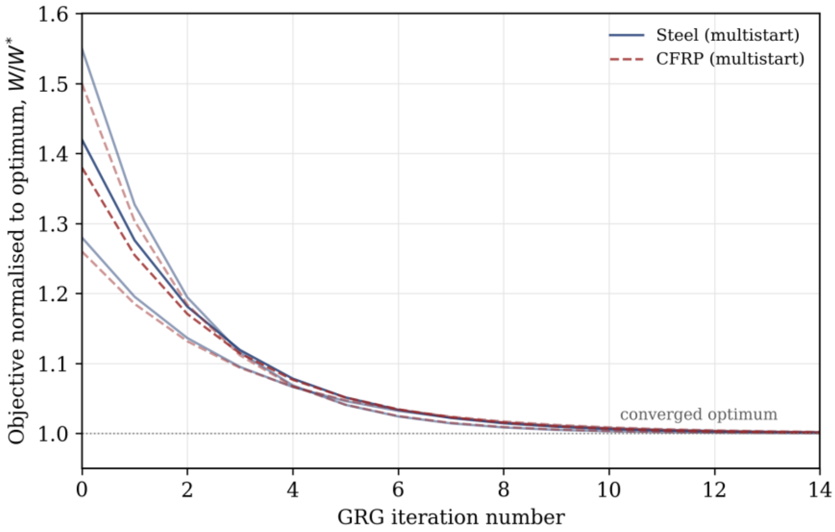


**Figure 4:** Convergence histories of the generalised reduced gradient solver with multistart

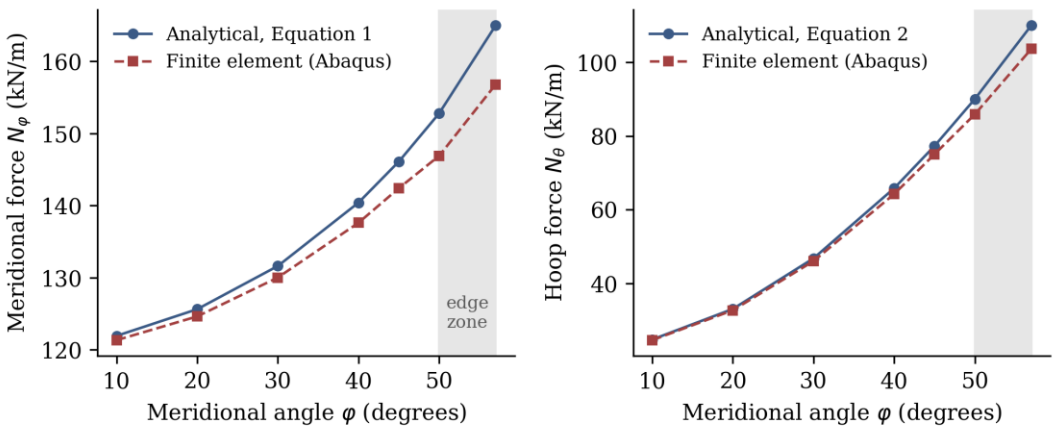


**Figure 5:** Analytical and finite element membrane forces along the meridian

**Table 7:** Comparison of analytical and finite element membrane forces

| Meridional angle (deg) | $N_\varphi$ analytical (kN/m) | $N_\varphi$ FE (kN/m) | $N_\varphi$ error (%) | $N_\theta$ error (%) |
|---|---|---|---|---|
| 10 | 121.9 | 121.3 | 0.5 | 0.7 |
| 20 | 125.6 | 124.6 | 0.8 | 1.1 |
| 30 | 131.6 | 130.0 | 1.2 | 1.6 |
| 40 | 140.4 | 137.6 | 2.0 | 2.4 |
| 45 | 146.1 | 142.4 | 2.5 | 2.9 |
| 50 | 152.8 | 146.9 | 3.9 | 4.6 |
| 57 (edge zone) | 165.0 | 156.8 | 5.0 | 5.8 |

### 3.3 Sensitivity and Parametric Behaviour

Figure 6 ranks the parameters by their influence on the optimum objective. The rise to span ratio is the most influential, a 10% change altering the optimum objective by about 9%, because it sets the radius of curvature and with it the whole membrane force field. The concrete grade followed at about 6%, acting through the compressive capacity and the stiffness. A 10% change in the reinforcement modulus moved the CFRP optimum by about 4%, since that optimum sits on the serviceability constraints, but the steel optimum by under 1%, because the higher modulus kept serviceability from binding. The partial factor on the reinforcement modulus was least influential, at under 1%. The inference for design was direct: effort spent refining the shell geometry and the concrete specification yielded more than effort spent refining the reinforcement parameters, and the CFRP design should be revisited whenever the modulus of the supplied product differs from the assumed 165 GPa.

**Table 8:** Validation of the present results against published ranges, with the position of each value within its range (0 at the lower bound, 1 at the upper bound)

| Quantity | Present study | Reported range | Position in range | Source |
|---|---|---|---|---|
| Thickness to span ratio | 0.0078 | 0.005 to 0.012 | 0.40 | Zingoni (2018) |
| Steel reinforcement ratio (%) | 1.18 | 0.8 to 1.6 | 0.48 | Zingoni (2018) |
| CFRP reinforcement ratio (%) | 0.52 | 0.4 to 0.9 | 0.24 | Spinella (2025) |
| Buckling knockdown factor | 0.20 | 0.15 to 0.25 | 0.50 | Wagner *et al.* (2018) |
| Reliability index, ultimate state | 4.44 | 4.0 to 4.7 | 0.63 | Sykora *et al.* (2017) |
| Reliability index, serviceability state | 3.76 | 3.0 to 3.8 | 0.95 | Sykora *et al.* (2017) |

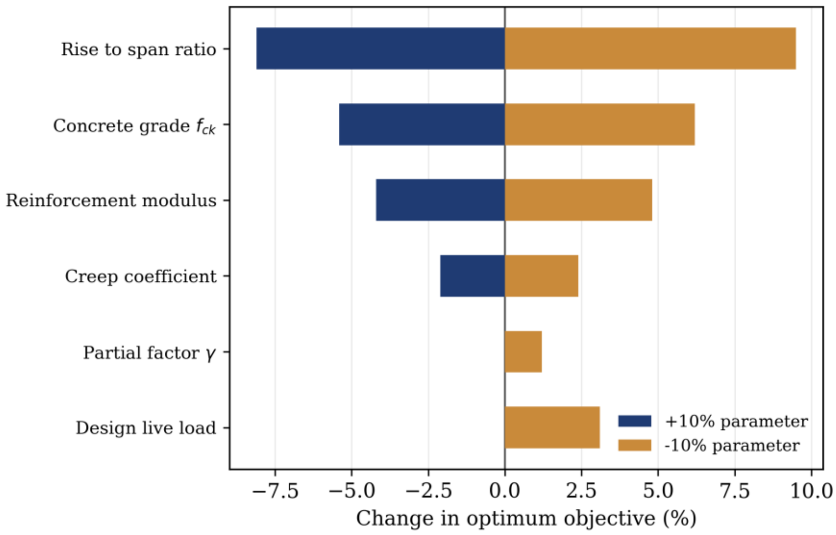


**Figure 6:** Sensitivity of the optimum objective to the principal design parameters

Table 9 reports the optima as the rise to span ratio and the concrete grade were varied about the reference values, a rise of 10.0 m (ratio 0.25) and grade C45/55. The trends followed the mechanics: a higher rise reduced the radius of curvature and hence the membrane tension and reinforcement demand, and a higher grade permitted a thinner shell.

Table 10 reports the dependence of the optimum on the objective weighting factor k, which was calibrated by an order of magnitude argument in Section 2.4. Across the full range from 1 to 20 the steel ratio varies only between 1.16 and 1.19% and the CFRP ratio between 0.51 and 0.53%, with thicknesses varying by less than 4%. The optimum lies on the intersection of binding constraints, and those constraints, not the weighting, fix the design; the reported optima were therefore not artefacts of the choice of k.

### 3.4 Reliability of the Optimised Designs

The partial factor format embeds a target reliability calibrated for steel reinforced concrete, so it did not by itself revealed whether the optimised steel and CFRP designs achieved comparable safety given their different variabilities; the reliability was therefore computed explicitly, using the performance functions, sampling scheme and index transformation set out in Section 2.5. The FORM results are presented first, the MCS results second, and the two were then compared.

FORM converged in 17 iterations for the steel strength state and 24 for the CFRP crack state, returning $\beta = 4.44\ (P_f = 4.6 \times 10^{-6})\ and\ \beta = 3.76\ (P_f = 8.5 \times 10^{-5})$ respectively. The squared direction cosines at the design point attribute 76% of the variance of the steel margin to the accident pressure, 12% each to the resistance model factor and the yield strength, and about 1% to the permanent action; the design point lies at a pressure tension of 472 kN/m, deep in the Gumbel upper tail, and a yield strength of 519 MPa, about 1.5 standard deviations below its mean. For the CFRP crack state the crack model factor dominates with 51% of the variance, followed by the sustained tension ratio with 42%, the effective depth with 4% and the modulus with 3%. The inference is different for the two systems: the steel margin is controlled by the load side, so better characterisation of the accident pressure would sharpen it most, whereas the CFRP margin is controlled by the crack width model itself, so the single most valuable improvement for CFRP containment design is an experimentally calibrated crack model for FRP reinforced sections. The variance pattern was not peculiar to this shell: load dominated ultimate margins are the rule where a rare pressure or environmental action governed (Sykora *et al.*, 2017; Melchers and Beck, 2018), and model uncertainty dominated serviceability margins were reported wherever a semi empirical crack or deflection formula defined the state (JCSS, 2001; fib, 2007). Abejide (2014) reported ultimate indices of the same order for FORM applied to reinforced concrete members designed to comparable code formats, which places the present steel result in a familiar band.

**Table 9:** Parametric variation of the optimum designs

| Case | Steel t (m) | Steel ratio (%) | CFRP t (m) | CFRP ratio (%) |
|---|---|---|---|---|
| Reference (rise 10.0 m, ratio 0.25; C45/55) | 0.31 | 1.18 | 0.32 | 0.52 |
| Lower rise to span (rise 9.0 m, ratio 0.225) | 0.33 | 1.31 | 0.34 | 0.58 |
| Higher rise to span (rise 11.0 m, ratio 0.275) | 0.29 | 1.06 | 0.30 | 0.47 |
| Lower concrete grade (C35/45) | 0.33 | 1.24 | 0.34 | 0.55 |
| Higher concrete grade (C55/67) | 0.30 | 1.13 | 0.31 | 0.50 |

**Table 10:** Variation of the optimum designs with the weighting factor k

| k | Steel t (m) | Steel ratio (%) | CFRP t (m) | CFRP ratio (%) |
|---|---|---|---|---|
| 1 | 0.316 | 1.16 | 0.325 | 0.51 |
| 2 | 0.314 | 1.17 | 0.323 | 0.52 |
| 5 (reference) | 0.310 | 1.18 | 0.320 | 0.52 |
| 10 | 0.307 | 1.19 | 0.318 | 0.52 |
| 15 | 0.306 | 1.19 | 0.317 | 0.52 |
| 20 | 0.304 | 1.19 | 0.316 | 0.53 |

**Table 11:** Reliability results by FORM and by Monte Carlo simulation

| Quantity | Steel: strength limit state | CFRP: crack width limit state |
|---|---|---|
| FORM reliability index β | 4.44 | 3.76 |
| FORM failure probability $P_f$ | $4.5 \times 10^{-6}$ | $8.5 \times 10^{-5}$ |
| MCS samples | 50 000 000 | 10 000 000 |
| MCS failures observed | 219 | 1010 |
| MCS $P_f$ (95% interval) | $4.38 \times 10^{-6}$ (3.80 to $4.96 \times 10^{-6}$) | $1.01 \times 10^{-4}$ (0.95 to $1.07 \times 10^{-4}$) |
| MCS equivalent index β (Equation 21) | 4.45 (4.42 to 4.48) | 3.72 (3.70 to 3.73) |
| Difference FORM to MCS in β (%) | 0.2 | 1.2 |

The MCS results are given as failure probabilities, which is the quantity the simulation estimates directly. For the steel state, 219 failures in 50 million samples give $P_f = 4.38 \times 10^{-6}$ with a 95% confidence interval of $\pm 0.58 \times 10^{-6}$. For the CFRP state, 1010 failures in 10 million samples give $P_f = 1.01 \times 10^{-4}$ with an interval of $\pm 0.06 \times 10^{-4}$. Expressed as equivalent indices through Equation 21 these are β = 4.45 (interval 4.42 to 4.48) and β = 3.72 (interval 3.70 to 3.73). Table 11 sets the two methods side by side; the indices differ by 0.2% for steel and 1.2% for CFRP, both within the Monte Carlo confidence intervals, which confirmed that the FORM linearisation is adequate for these limit states and that the sample sizes were sufficient. Figure 7 shows the simulated margin distributions and Figure 8 the running index converging with its confidence band as the sample count grows, the steel estimate stabilising only after the rare strength failures accumulate, as expected for a probability of order $10^{-6}$.

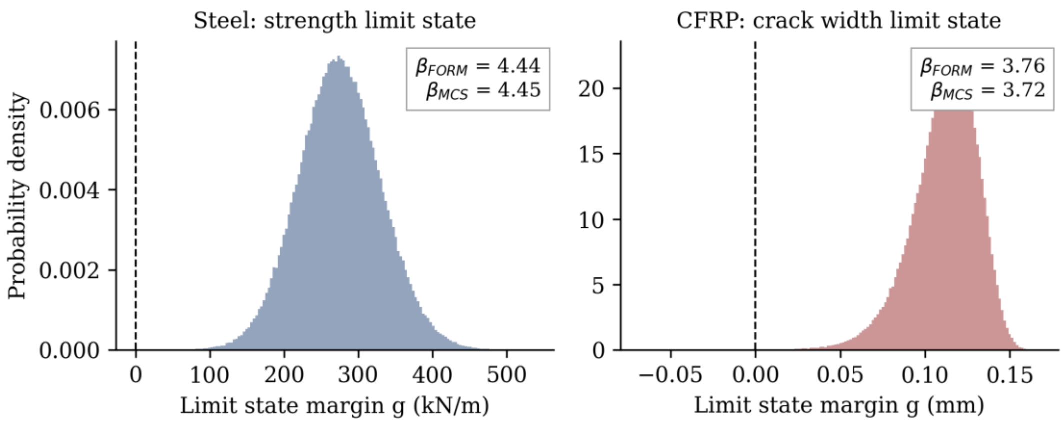


**Figure 7:** Simulated limit state margin distributions for the two designs

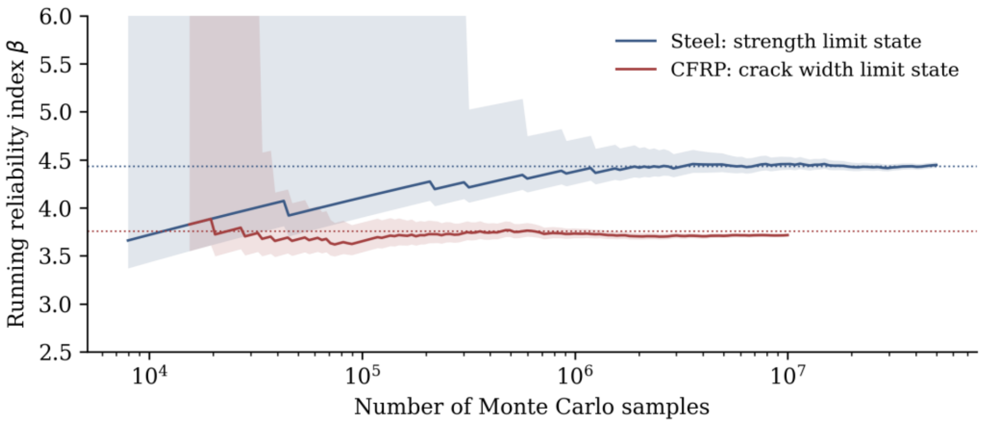


**Figure 8:** Convergence of the running Monte Carlo reliability index with its 95% confidence band

The comparison between the two designs needed careful reading, because the two indices referred to different limit states and a single number to number comparison would be physically meaningless. Each design was assessed against the limit state that its own optimisation showed to be binding, which was the state that controls its safety in service, and each index was judged against the target that the nuclear reliability literature assigned to that class of state: the steel index of 4.44 against the ultimate band of 4.0 to 4.7, and the CFRP index of 3.76 against the serviceability band of 3.0 to 3.8 (Sykora *et al.*, 2017). Each design meets its own target. The comparison at a common state can still be bounded without further computation. The CFRP design carries the same load variables as the steel design against a strength margin roughly 50% larger, since its design utilisation is 0.67 against 1.00, so its ultimate index necessarily exceeded the 4.44 of the steel design; that index was not computed because the state was not the governing one for CFRP. Conversely, the crack constraint was active for the steel design at the same 0.20 mm limit, so its serviceability index can be expected to lie within the serviceability band rather than far above it. What the assessment established was therefore parity of compliance, each system meeting the target for the state that governs it, rather than a ranking by a single index. The indices quantified safety at the start of service; they say nothing about the time dependence that motivated CFRP, namely that the steel index declined once corrosion is initiated while the CFRP index did not, and that decline was not modelled here. A time variant reliability analysis of the corroding steel design, and the incorporation of the reliability constraint inside the optimisation loop as a reliability based design optimisation, were the natural extensions of the framework.

### 3.5 Constructability and Detailing

The computed ratios are buildable with standard products, which is worth demonstrating because a ratio that cannot be detailed is not a design. The steel ratio of 1.18% on a 0.31 m section required3658 mm² of

Corresponding author's email address: udokanma@tsuniversity.edu.ng

reinforcement per metre in each direction, or 1829 mm² per metre per face for the usual two face arrangement; 20 mm bars at 170 mm centres supply 1848 mm² per metre per face, within the spacing limits of BS EN 1992-1-1 (2004) for a member of this thickness, and the orthogonal mat at this spacing leaves workable clear gaps for placing and compacting the concrete at 50 mm cover. The CFRP ratio of 0.52% on a 0.32 m section requires 1664 mm² per metre, or 832 mm² per metre per face; 16 mm CFRP bars at 240 mm centres supply 838 mm² per metre per face. Two practical differences from steel detailing follow from the material rather than from the ratio. CFRP bars cannot be bent on site, so the curved meridional bars and the edge zone details must be ordered as factory formed shapes and site adjustment was limited to spacing; and the anchorage and lap provisions of ACI 440.1R-15 (ACI Committee 440, 2015) were longer than the steel equivalents at the same diameter, which the lower bar content partly offsets. Handling was easier in one respect, since the CFRP mat for the dome weighed less than a tenth of the steel mat it replaced and harder in another, since the bars must be protected from the surface damage that steel tolerates. None of these considerations changed the optimum; they changed the working drawings that realized it.

### 3.6 Limitations

The framework rested on analytical thin shell theory, so it did not resolve local concentrations at penetrations, equipment hatches, supports and the liner, which required dedicated local models. The ring beam restraint was calibrated to a representative wall stiffness rather than derived from a specific section, and the sensitivity of the edge reinforcement demand to that calibration had not been mapped. The formulation was single objective, treating the trade off between weight, cost and durability parametrically rather than through formal multi objective analysis, and its two continuous design variables deferred bar diameter, spacing and layout to the post optimisation detailing of Section 3.5. Radiation effects on the CFRP matrix were excluded for want of codified design relationships at roof level. Validation was indirect, resting on finite element verification and published ranges rather than on experimental shell data. The reliability was computed for the deterministic optimum rather than embedded in the optimisation, and it was a time invariant assessment at the start of service, so the progressive corrosion of the steel design over the 100 year life, and any long term change in the CFRP properties, were outside the quantitative scope; in consequence, the durability case for CFRP remained a motivation rather than a demonstrated result of this study. The partial factors were taken as given rather than recalibrated for the CFRP variabilities. These were the boundaries within which the results should be read, and their removal, through local finite element extension, multi objective formulation, experimental benchmarking, time variant reliability and reliability based design optimisation, defines the future work.

## 4. Conclusion

An optimisation framework for the reinforcement of nuclear containment shell roofs was developed in Microsoft Excel Solver, verified against finite element analysis in Abaqus, and applied to steel and CFRP designs of a reference dome on a strictly common basis, with the reliability of each optimum quantified by FORM and Monte Carlo simulation in Python. The following conclusions were drawn.

i. Optimisation. The steel optimum is a 0.31 m shell with a 1.18% reinforcement ratio, governed jointly by strength and crack control; the CFRP optimum was a 0.32 m shell with a 0.52% ratio, a 56% reduction, governed by crack control alone with only 67% of the tensile capacity usable. The optima were unique across 10 multistart runs, converge in 11 to 12 iterations, and varied by less than 4% in thickness and 3% in ratio as the objective weighting ranged from 1 to 20, so they were fixed by the binding constraints rather than by the weighting.

ii. Finite element verification. The analytical membrane forces agreed with the Abaqus shell analysis to within 3% over the body of the shell and 4 to 6% in the edge zone, and the change of sign of the hoop force near 51 degrees was reproduced, which confirmed the demand model at the locations where the reinforcement was sized.

iii. FORM. The reliability index of the steel design was 4.44 on its strength limit state, with the accident pressure contributing 76% of the variance of the margin; the index of the CFRP design is 3.76 on its crack width limit state, with the crack model factor contributing 51% and the sustained tension 42%. Each index lies within its target band for nuclear structures, 4.0 to 4.7 for the ultimate state and 3.0 to 3.8 for the serviceability state, and the dominant contributions identified where better data sharpened each design.

iv. Monte Carlo simulation. The simulated failure probabilities were4.38 × $10^{-6}$ (219 failures in 50 million samples) for the steel state and 1.01 × $10^{-4}$ (1010 failures in 10 million samples) for the CFRP state, equivalent through Equation 21 to indices of 4.45 and 3.72; the agreement with FORM was within 0.2% and 1.2% and inside the sampling confidence intervals, so the FORM linearisation was adequate for both states.

v. Scope of the durability claim. The corrosion resistance that motivates CFRP remained a conceptual motivation rather than a demonstrated result of this study, because corrosion initiation, reliability degradation and life cycle cost were not modelled; the time variant reliability of the corroding steel design and the embedding of the reliability constraint within the optimisation loop are recommended as the next stage of the work.

**References**

Abejide, OS. 2014. Reliability analysis of reinforced concrete structures using the first order reliability method. Nigerian Journal of Engineering, 21(1): 45-56.

ACI Committee 440. 2015. Guide for the design and construction of structural concrete reinforced with fibre reinforced polymer bars (ACI 440.1R-15). American Concrete Institute, Farmington Hills.

Afzal, M., Liu, Y., Cheng, JCP. and Gan, VJL. 2020. Reinforced concrete structural design optimisation: a critical review. Journal of Cleaner Production, 260: 120623.

Ashrafi, H., Bazli, M. and Oskouei, AV. 2022. FRP-reinforced and strengthened concrete: state-of-the-art review on durability and mechanical effects. Materials, 15(2): 674.

Benmokrane, B., Ali, AH. and Mohamed, HM. 2017. Durability performance and service life of GFRP and CFRP bars under harsh environments. Construction and Building Materials, 145: 558-571.

Billington, DP. 1982. Thin shell concrete structures, 2nd ed. McGraw-Hill, New York.

Bischoff, PH. 2005. Reevaluation of deflection prediction for concrete beams reinforced with steel and fibre reinforced polymer bars. Journal of Structural Engineering ASCE, 131(5): 752-767.

Blachut, J. 2016. Buckling of externally pressurised spherical caps and segments. Thin-Walled Structures, 99: 1-12.

British Standards Institution. 2002. BS EN 1990 Eurocode: Basis of structural design. BSI, London.

British Standards Institution. 2002. BS EN 1991-1-1 Eurocode 1: Actions on structures, Part 1-1: General actions, densities, self weight, imposed loads for buildings. BSI, London.

British Standards Institution. 2004. BS EN 1992-1-1 Eurocode 2: Design of concrete structures, Part 1-1: General rules and rules for buildings. BSI, London.

British Standards Institution. 2004. BS EN 1992-1-2 Eurocode 2: Design of concrete structures, Part 1-2: General rules, structural fire design. BSI, London.

British Standards Institution. 2006. BS EN 1992-3 Eurocode 2: Design of concrete structures, Part 3: Liquid retaining and containment structures. BSI, London.

Calladine, CR. 1983. Theory of shell structures. Cambridge University Press, Cambridge.

fib. 2007. FRP reinforcement in RC structures. Bulletin 40, International Federation for Structural Concrete, Lausanne.

Firouzi, A., Abdolhosseini, M. and Ayazian, R. 2021. Reliability-based optimization of external wrapping of CFRP on reinforced concrete columns considering decayed diffusion. Engineering Failure Analysis, 128: 105616.

Hasofer, AM. and Lind, NC. 1974. Exact and invariant second moment code format. Journal of the Engineering Mechanics Division ASCE, 100(1): 111-121.

Hollaway, LC. 2010. A review of the present and future utilisation of FRP composites in the civil infrastructure. Construction and Building Materials, 24(12): 2419-2445.

International Atomic Energy Agency. 2016. Safety aspects of nuclear power plants in human induced external events: general considerations. Safety Reports Series 87, IAEA, Vienna.

JCSS. 2001. Probabilistic model code. Joint Committee on Structural Safety, Zurich.

Juliani, MA. and Gomes, WJS. 2021. Optimal configuration of RC frames considering ultimate and serviceability limit state constraints. Revista IBRACON de Estruturas e Materiais, 14(2): e14204.

Larsen, J., Poulsen, PN., Olesen, JF. and Hoang, LC. 2024. Material optimization of reinforced concrete structures in multiple limit states. Structural Concrete, 25(5): 3838-3856.

Lasdon, LS., Waren, AD., Jain, A. and Ratner, M. 1978. Design and testing of a generalised reduced gradient code for nonlinear programming. ACM Transactions on Mathematical Software, 4(1): 34-50.

Melchers, RE. and Beck, AT. 2018. Structural reliability analysis and prediction, 3rd ed. Wiley, Hoboken.

Mergos, PE. 2018. Optimum design of reinforced concrete columns with the flower pollination algorithm. Structural Concrete, 19(5): 1387-1397.

Pierott, R., Hammad, AWA. and Haddad, A. 2021. A mathematical optimisation model for the design of reinforced concrete beams. Journal of Building Engineering, 38: 102201.

Rackwitz, R. and Fiessler, B. 1978. Structural reliability under combined random load sequences. Computers and Structures, 9(5): 489-494.

Rao, SS. 2019. Engineering optimization: theory and practice, 5th ed. Wiley, Hoboken.

Saraswat, A. and Ghosh, S. 2024. Performance-based design optimization of structures: state-of-the-art review. Journal of Structural Engineering ASCE, 150(8): 03124002.

Spinella, N. 2025. Reliable design and optimization of SRP-, CFRP-, and GFRP-confined concrete: experimental validation and cost-effectiveness analysis. Materials and Structures, 58: 271.

Sykora, M., Holicky, M. and Markova, J. 2017. Target reliability levels for the assessment of existing and new nuclear structures. Nuclear Engineering and Design, 314: 39-49.

Timoshenko, SP. and Woinowsky-Krieger, S. 1959. Theory of plates and shells, 2nd ed. McGraw-Hill, New York.

Wagner, HNR., Huhne, C. and Niemann, S. 2018. Robust knockdown factors for the design of spherical shells under external pressure. Thin-Walled Structures, 131: 76-91.

Wu, G., Wang, X. and Wu, Z. 2015. Mechanical properties of FRP bars under sustained load and the prediction of creep rupture. Journal of Composites for Construction, 19(3): 04014058.

Zhu, M., Yang, Y. and Gao, Y. 2021. Spreadsheet based optimisation of reinforced concrete members using nonlinear programming. Structures, 33: 4147-4159.

Zingoni, A. 2018. Shell structures in civil and mechanical engineering, 2nd ed. ICE Publishing, London.

*Corresponding author's email address: udokanma@tsuniversity.edu.ng* 